AGU100 ADVANCING EARTH AND SPACE SCIENCE

Geophysical Research Letters

RESEARCH LETTER
10.1029/2019GL082629

Countrywide Observations of Plate Spreading and Glacial Isostatic Adjustment in Iceland Inferred by Sentinel-1 Radar Interferometry, 2015–2018

Vincent Drouin[1,2] **and Freysteinn Sigmundsson**[1]

[1]Nordic Volcanological Center, Institute of Earth Sciences, University of Iceland, Reykjavik, Iceland, [2]National Land Survey of Iceland, Akranes, Iceland

Abstract East-west and vertical ground velocities for 2015–2018 are retrieved over 81% of Iceland from Sentinel-1 radar interferometry, using satellite images from six different tracks. Only summertime images are considered, to avoid snow cover. Average line-of-sight velocity fields for 2015–2018 for each track are estimated using a simple approach: single master interferometry time series together with a linear component estimation for each pixel. The line-of-sight velocity fields are combined and their signal is decomposed to extract approximate east (near-East) and approximate vertical (near-Up) velocities. Only pixels passing a coherence and outlier criteria are considered, resulting in 81% coverage of Iceland. The 19% of missing coverage is mostly glaciers and farmland. We find a general agreement between the near-East velocity field and a revised plate spreading model, and the near-Up velocity field and a glacial isostatic adjustment model. Models and their residuals suggest a difference in rheology between the rift zones in Iceland.

Key Points:
- Deformation information over 81% of Iceland is derived from InSAR time-series analysis
- Plate spreading dominates long-wavelength east-west displacements; GIA dominates long-wavelength vertical displacements
- Models and residuals suggest spatially variable rheology beneath Iceland

Supporting Information:
- Supporting Information S1

Correspondence to:
V. Drouin,
vd@hi.is

Citation:
Drouin, V., & Sigmundsson, F. (2019). Countrywide observations of plate spreading and glacial isostatic adjustment in Iceland inferred by Sentinel-1 radar interferometry, 2015–2018. *Geophysical Research Letters*, *46*, 8046–8055. https://doi.org/10.1029/2019GL082629

Received 28 FEB 2019
Accepted 8 JUL 2019
Accepted article online 15 JUL 2019
Published online 29 JUL 2019

1. Introduction

Iceland is continuously deforming due to multiple processes, including plate spreading, glacial isostatic adjustment (GIA) and more local volcanic and geothermal processes. The plate boundary between the North American and Eurasian Plates runs through Iceland (Figure 1). About 11% of the island is covered by glaciers of varying size (Björnsson & Pálsson, 2008). The plate divergence is witnessed clearly in geological and rift zone structures created since the formation of the oldest rocks in Iceland, about 16 million years ago. Ground deformation studies using Global Positioning System (GPS) geodetic measurements since 1986 also show well the plate spreading (e.g., Sigmundsson, Einarsson, et al., 2018). Interferometric analysis of synthetic aperture radar (InSAR) images from various satellites have been carried out in Iceland, with data available since 1992, providing constraints on the plate spreading deformation signals (Pedersen et al., 2009; Vadon & Sigmundsson, 1997). Plate divergence amounts to 17–19 mm/year in direction N(105–110)°E, accommodated by about 50- to 150-km-wide zones.

Another major source of countrywide crustal deformation in Iceland is GIA in response to thinning and retreat of Icelandic ice caps after 1890, since the end of the Little Ice Age. Multiple studies have shown that a large part of Iceland is undergoing uplift with rates higher than 25 mm/year, as well as horizontal displacements of more than a few millimeters per year in response to the ice retreat. This was well observed in countrywide GPS observations from 1993–2004 (Árnadóttir et al., 2009) and also prior to that in more local GPS studies (e.g., Pagli et al., 2007). GIA around the largest ice cap in Iceland, Vatnajökull, has also been studied with InSAR (Auriac et al., 2013, 2014). Most previous studies have relied on an Earth model structure consisting of a Maxwell viscoelastic material overlain by an elastic plate, of uniform or varying properties. Assuming uniform viscosity below an elastic layer, the inferred models have viscosity in the range 4–10 $\times 10^{18}$ Pa/s, and an elastic layer thickness in the range 15–40 km (Auriac et al., 2013; Árnadóttir et al., 2009).

Extensive studies of deformation due to magmatic processes (Sigmundsson, Parks, et al., 2018), and of ground deformation in geothermal areas (e.g., Drouin et al., 2017; Juncu et al., 2017; Keiding et al., 2010; Parks et al., 2018) have been carried out.

InSAR has played a role in the studies of all these processes. Various satellites have been used, including ERS1 and ERS2, Envisat, TerraSAR-X, COSMO-SkyMed, and Radarsat. We present results from

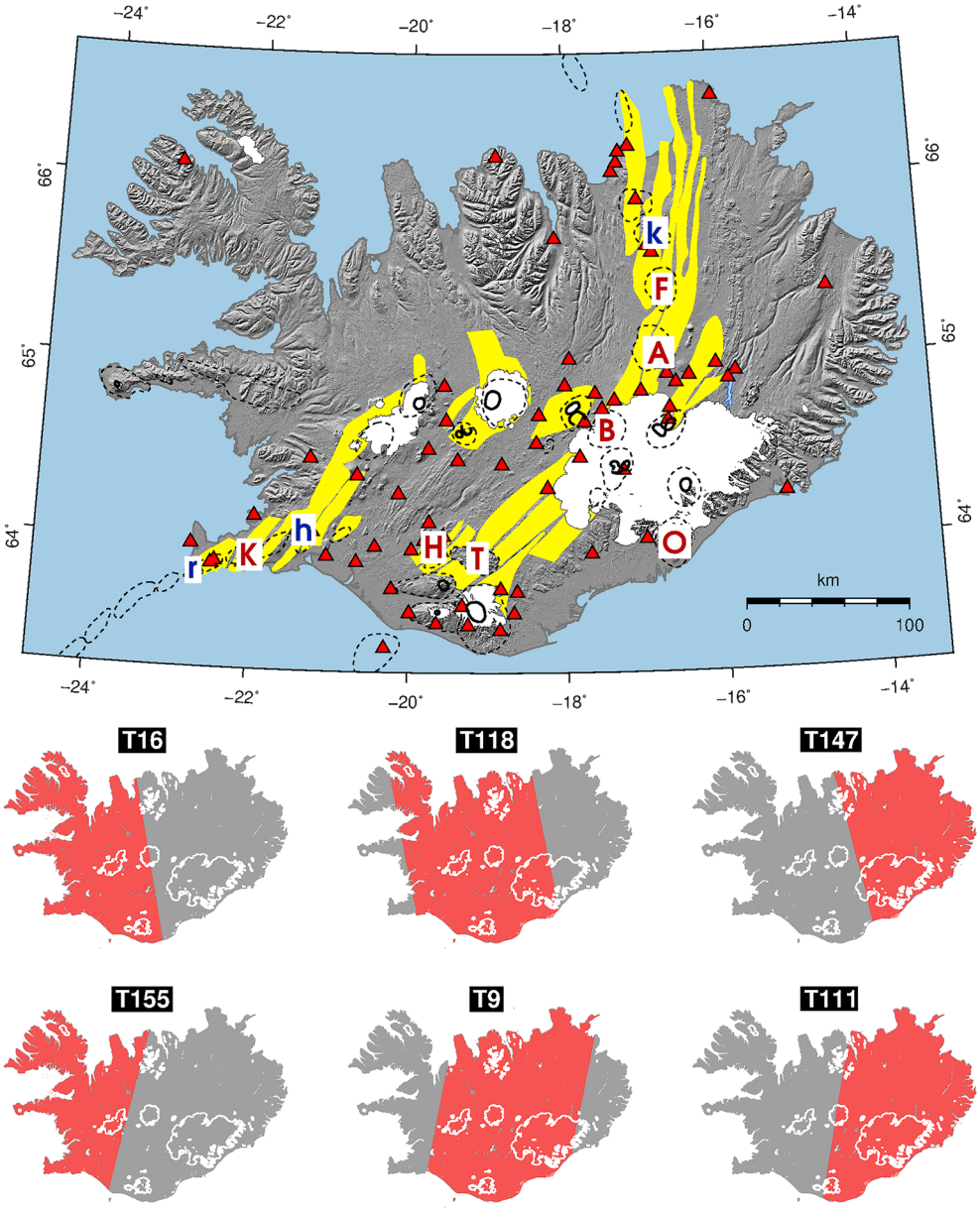

Figure 1. (upper) Map of Iceland showing ice caps (white), outlines of central volcanoes (dashed lines), calderas (thick lines), fissure swarms (yellow), and shaded topography. For geological layers, see Sigmundsson, Einarsson, et al. (2018, and references therein). Red triangles show continuous Global Positioning System sites. Selected geothermal areas are indicated in blue: Reykjanes (r), Hengill (h), and Krafla (k). Selected volcanoes are indicated in red: Krísuvík (K), Hekla (H), Torfajökull (T), Bárðarbunga (B), Öræfajökull (O), Askja (A), Fremri-námar (F), and Krafla (k in blue). (lower) Coverage of the six selected Sentinel-1 tracks (red) over Iceland (gray). White lines show glacier outlines.

interferometric studies using images from the Sentinel-1A and Sentinel-1B satellites, covering all of Iceland. The first 4 years of summertime images available from the Sentinel-1A and Sentinel-1B satellites are used. Our study differs from previous InSAR studies in Iceland in that it is the first InSAR study to cover the whole island.

2. Data

2.1. Sentinel-1 Images

The first Sentinel-1A interferometric-wide (IW) images over Iceland were acquired in late fall 2014. Images were collected initially with an acquisition rate of 12 days, which was reduced to 6 days in early 2017 with the addition of the Sentinel-1B satellite. Parts of Iceland are covered with snow from early fall until late spring.

Consequently, only summer images are generally useful for interferometric purposes. Therefore, we only consider images acquired in summer, from mid-June to late September. The use of the same time period each year ensures that effects of the annual cycle in load-induced deformation in Iceland (Drouin et al., 2016) are minimal.

Iceland is about 500 km wide from east to west and 300 km wide from north to south. A Sentinel-1 IW image is composed of three subswaths, each about 80 km wide, with a total width of about 240 km. Pixel spacing in images is about 2.3 m in range and 14.1 m in azimuth, while the spatial resolution (measure of the system's ability to distinguish between adjacent targets) is about 2.7–3.5 m in range and 22 m in azimuth (Bourbigot et al., 2016). To provide full coverage of Iceland from both ascending and descending orbits, we selected three ascending tracks (T16, T118, and T147) and three descending tracks (T155, T9, and T111; Figures 1 and S1 in the supporting information). Along the same orbit track, two to four IW images are necessary to cover Iceland from north to south. The total number of summer acquisitions for each track (both 1A and 1B) range from 48 to 53. Having both ascending and descending coverage of the same area allows us to estimate the approximate east displacement (near-East) and approximate vertical displacement (near-Up) components.

2.2. Analysis

Interferograms were generated using the InSAR Scientific Computing Environment software version 2.2.0 developed jointly by the Jet Propulsion Laboratory, Caltech, and Stanford University, and distributed by the Western North America Interferometric Synthetic Aperture Radar consortium (Rosen et al., 2012). This software has the capability to stitch subswaths together as well as images from the same orbit track in a single process. We were therefore able to generate 240-km-wide interferograms covering Iceland from north to south.

In order to improve the signal to noise ratio, interferograms are multilooked by 19 in range and 7 in azimuth (InSAR Scientific Computing Environment default values), resulting in about 45-m × 100-m pixels. A Goldstein-Werner power spectral smoothing filter with a strength of 0.5 is also applied during processing (Goldstein & Werner, 1998). Topographic fringes are removed using an intermediate TanDEM-X digital elevation model (DEM) resampled to ~50-m grid, with no-data gaps filled with values from an ASTER DEM. Final interferograms are geocoded to the DEM grid and therefore also have a pixel size of about 50×50 m^2.

Justification of TS analysis to mitigate random atmospheric noise !

Changes in the atmosphere between two SAR acquisitions cause noise, which can generate one or more interferometric fringes. Individual sources of long-term deformation in Iceland typically generate less than one fringe in a 1-year Sentinel-1 interferogram (<28 mm/year): GIA is less than 30 mm/year in most areas, plate spreading is below 20 mm/year, and local deformation signals from volcanic and geothermal sources are often of this magnitude or less. In our case, with only four years of data, the signal to noise ratio is therefore low in each interferogram. However, plate spreading and GIA deformation signals in Iceland are reasonably linear with time, while atmospheric disturbances are closer to random noise. We used time series analysis to infer average 2015–2018 ground velocities in order to mitigate the atmospheric noise and enhance the deformation signal.

VIsual inspection

We used the following approach to derive the 2015–2018 line-of-sight (LOS) velocity field for each track: (i) Interferograms are formed with the same master image. The master image is from August 2017 to minimize the temporal decorrelation with images in 2015 and 2018. For each track, we obtained about 50 interferograms. (ii) All interferograms are referenced to the same area to form a stack. (iii) Interferograms seriously contaminated by noise as judged by visual inspection (debursting errors, extreme atmospheric noise) are removed from the stack. (iv) For each pixel in the resulting stack of interferograms, a linear trend is estimated and the value is written in the corresponding pixel of the velocity field.

The resulting 2015–2018 average LOS velocity fields are shown in Figures S2–S7 in the supporting information (see Acknowledgements for data access). They are in good agreement with the deformation observed by the network of continuous GPS (cGPS) stations in Iceland. The cGPS data have been analyzed at the University of Iceland using GAMIT/GLOBK 10.6 (Herring et al., 2015). Site positions were evaluated in the ITRF2014 reference frame using over 100 worldwide reference stations. East, North, and Up velocities were derived from the resulting time series by extracting the linear component of the deformation from early summer 2015 to early fall 2018. These velocities were then referenced to the Eurasian plate (Altamimi et al., 2017) and converted to LOS velocities using heading and incidence angle information for each InSAR track.

2.3. Decomposition Into Near-East and Near-Up Velocities

Due to the near-polar orbits of SAR satellites orbiting around the Earth, InSAR is mostly sensitive to vertical displacements and horizontal displacements in the east direction. For example, for a satellite heading of N191°E and an incidence angle of 38° (average Sentinel-1 values for a descending track), North displacements need to be more than 5 times larger than East displacements, or to be more than 6 times larger than Up displacements, to generate the same amount of LOS displacement. Iceland is not subject to large north-south displacements, in general, as most of the plate spreading is approximately east-west oriented and the GIA is dominated by vertical movements. By combining the LOS signal of an ascending track and a descending track (both right looking), it easy to discriminate between East and Up displacements as the East displacement changes sign depending on the satellite point of view while the Up displacement sign is the same. Extracting the north component of displacement is very difficult due to low sensitivity caused by the near-polar orbit of the satellite, even with three or more tracks covering the same area. Therefore, we only inverted for the East and Up displacements, while the contribution of North displacements to the LOS signal were considered insignificant. However, this can have a small influence on the extracted East and Up displacements, so we refer to them as near-East and near-Up displacements.

The inferred LOS velocity fields from all the tracks are combined and decomposed into a single near-East velocity field and a single near-Up velocity field for all of Iceland. This is possible because every part of the country is covered by at least one ascending track and one descending track (see Figure S1 in the supporting information for overlap between tracks). We used the following approach to decompose the LOS velocities in near-East and near-Up velocities: (i) LOS velocity field from each satellite track is referenced to the continuous GPS network of Iceland, with the GPS velocities referenced to the Eurasian plate. This is done by minimizing the difference between the InSAR LOS velocities and the LOS velocities derived from the 2015–2018 cGPS observations, by applying a constant shift to each LOS velocity field. (ii) Each LOS velocity field is resampled to the same grid that covers all of Iceland (the ~50-m DEM grid). Incidence and heading information for each track is also resampled to the same grid. (iii) For each pixel, we calculate the unit vector from ground to satellite for each track covering this pixel. (iv) For each pixel, all the unit vectors and associated LOS velocities are used in a least square inversion for near-East and near-Up values. (v) Only pixels with an average coherence over 0.4 are kept. The average is computed using the coherence of interferograms where the slave image is not in the same year as the master (2017), in order to ensure we are evaluating the long-term coherence. (vi) Pixel outliers are identified and removed by searching for pixels with more than a 5-mm/year difference between the near-East grid and a filtered version of it, using a 9×9 pixels median filter. The near-Up grids are treated in the same way. Pixel outliers found in either the near-East or near-Up grids are removed from both grids. Eighty-one percent of the pixels covering Iceland pass the selection criteria. We only considered images acquired in summer to avoid snow cover. Therefore, the 19% of missing coverage are areas that experience too much surface changes between summers. In Iceland, these areas are mostly glaciers, farmland, and unconsolidated sand deserts.

Resulting near-East and near-Up velocity fields are shown in Figures 2a and 2b, respectively (see Acknowledgements for data access). We clearly observe two countrywide deformation fields: plate spreading in the near-East component and GIA in the near-Up component. Minor discontinuities in the velocity fields are visible at boundaries between areas covered by a different number of tracks, but they are relatively small when compared to the observed deformation. Note that no smoothing or constraint is applied to the solution, each pixel is inverted independently.

3. Model

3.1. GIA

GIA is the main source of vertical deformation at the regional scale in Iceland, with thinning of the ice caps since 1890 generating upward velocities of up to 20–30 mm/year at the margins of glaciers. The GIA signal was first observed countrywide in Iceland with campaign GPS measurements from 1993–2004 (Árnadóttir et al., 2009). That study considered a model consisting of an elastic layer overlying a Maxwell viscoelastic half-space, with glaciers thinning at different rates based on historical mass balance measurements. A similar approach was later used by Auriac et al. (2013, 2014) with a finite element model and using InSAR velocities from the edges of the Vatnajökull ice cap in addition to GPS data.

We compare our observations to a GIA model by Auriac (2014), which uses a refined glacier thinning model compared to earlier studies, and a three-layer Earth model: a top 1-km-thick elastic layer with Young's

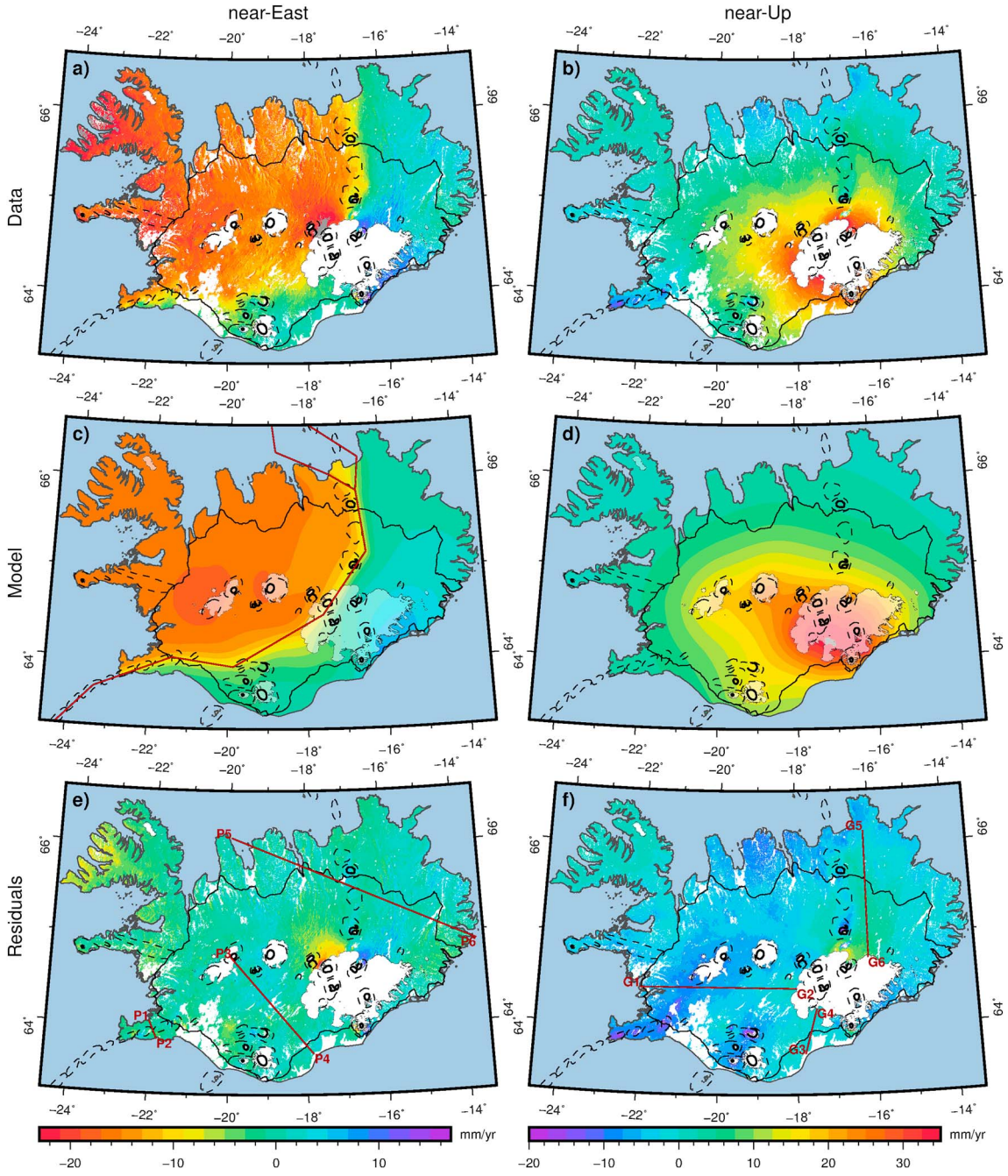

Figure 2. (a) Near-East and (b) near-Up velocity fields derived from the decomposition of line-of-sight velocities from interferometric analysis of six synthetic aperture radar tracks. (c) East velocity field derived from plate spreading and GIA models. Red lines show plate boundary segments. (d) Up velocity field derived from GIA model. (e) Near-East and (f) near-Up residuals after removal of the model velocities. See text for explanations. GIA = glacial isostatic adjustment.

modulus $E = 14$ GPa and Poisson's ratio $\nu = 0.17$, an intermediate 21-km-thick elastic layer with $E = 74$ GPa and $\nu = 0.25$ and a viscoelastic layer with $E = 74$ GPa, $\nu = 0.25$ and viscosity $\eta = 8.4 \times 10^{18}$ Pa s. Campaign GPS data in the Northern Volcanic Zone (NVZ) showed the need to apply a scale factor of 1.8 to the modeled GIA vertical velocities (Drouin et al., 2017). We explore this possibility by running a series of scaled versions of the Auriac (2014) model, to find the best fitting one. We tried a scale factor from 0.8 to 2.0 with steps of 0.1 to cover a wide range of possibilities from underestimation to overestimation of the GIA by the model. Profiles across the residual near-Up velocity fields after removal of the GIA give an indication of different best fitting scale factors (Figure 3, right). Profiles were selected to be orientated toward the main GIA source and have maximum length while not crossing a plate boundary. The profile west and south (of Vatnajökull)

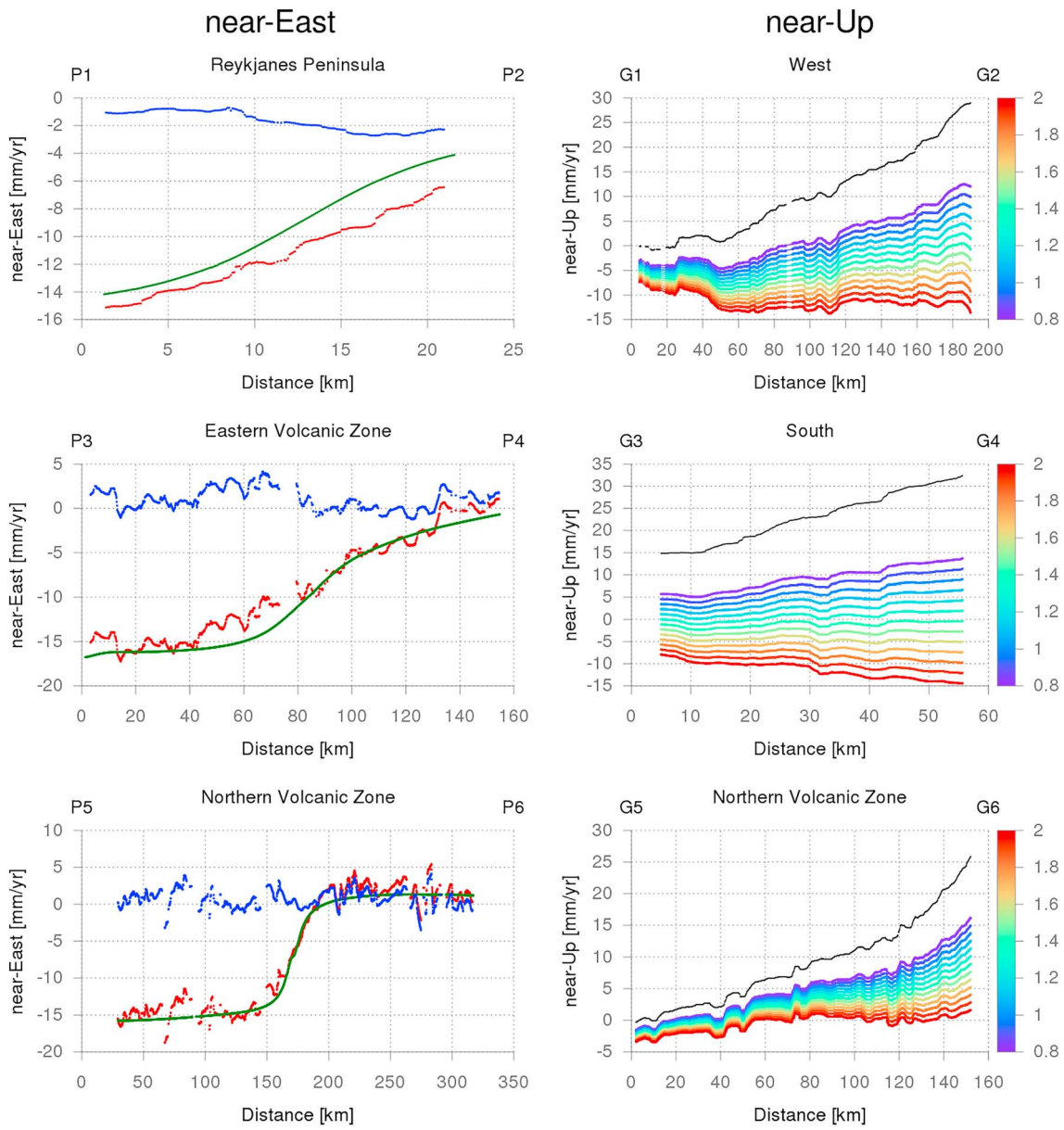

Figure 3. (left column) Profiles across near-East velocity fields (section 3.2). Red lines show data (Figure 2a), green lines show the plate boundary model (Figure 2c), and blue lines show residuals (Figure 2e). (right column) Profiles across near-Up residual velocity fields (Figure 2f). Color scales indicate the scale factor applied to the original velocity field modeled by Auriac (2014). Black lines show the uncorrected velocity field (Figure 2b). A boxcar filter is applied to all profiles to minimize noise.

shows a best fit at a scale factor of about 1.2–1.4, while the NVZ profile shows a best fit at a scale factor of about 1.8–2.0. The standard deviation of the entire near-Up velocity field has a minimum (3.38 mm) for a scale factor of 1.3–1.4, compared to the standard deviation of 7.36 mm for the uncorrected velocity field. Vertical velocities as predicted by the model scaled by 1.4 are shown in Figure 2d.

3.2. Plate Spreading

Plate spreading is the main source of horizontal deformation at a regional scale in Iceland. Here we use a back slip model to predict plate boundary deformation with a smooth transition in horizontal velocities from one plate to the other. A back slip model assigns half the plate motion to each side of the plate boundary, with superimposed velocities predicted by a vertical dislocation from the surface to a locking depth, closing at a rate equal to the plate motion (e.g., Metzger et al., 2011). The location of spreading segments and variable locking depth in the back slip model was initially extracted from three studies focused on specific segments

of the plate boundary: Metzger and Jónsson (2014), Drouin et al. (2017), and Geirsson et al. (2012). The spreading rate is 17.4 mm/year in the N292°E direction relative to the stable Eurasian plate (Drouin et al., 2017). Table S1 in the supporting information shows the parameters used for each plate boundary segment from earlier studies.

We also considered the horizontal deformation caused by GIA and corrected our near-East velocities for the horizontal velocities predicted by the Auriac (2014) model. We searched for a best fitting horizontal GIA scale factor, different to the vertical GIA scale factor, as done similarly by Drouin et al. (2017), as the simplifying model assumptions and nonmodeled three-dimensional viscosity variations may have significantly different influence on vertical and horizontal model displacements (e.g., Latychev et al., 2005). We evaluated scale factors varying from 0.5 to 3.0 with steps of 0.1. We found that residuals have a minimum for a scale factor of 2.6. Visual inspection of residuals also shows that scale factors between 2 and 3 explain best the near-East velocities on the Eurasian plate north and south of Vatnajökull.

Using the near-East displacement corrected from the GIA influence, we searched for refined plate boundary parameters. We initially resampled the near-East velocity to a 2 × 2-km grid (median resample) and applied a median filter (5 pixels width) to it. This allowed us to minimize small-scale deformation signals in the data while retaining the information about the plate spreading. We then sampled 300-km-wide profiles across the resulting grid. They are centered on the plate boundary segments (Table S1) and spaced every 2 km along the North direction. They are oriented N315°E in the south and along the plate spreading direction (N292°E) in the rest of the country. For each of the profiles, we did a grid search for the locking depth (from 1 to 15 km, 200-m steps), the plate velocity (from 16 to 22 mm/year, 0.5-mm/year steps), and the East location (from 30 km west to 30 km east of the initial segments, 1-km steps) of an infinitely long back slip segment orientated north-south. We minimized the standard deviation of the residuals. We ended with 196 points (one along each profile) giving the location of the central axis of the plate boundary, its locking depth, and the plate velocity (see Figure S8 in the supporting information). Points falling beneath an ice cap were not considered. We created an updated plate boundary model by extracting the location plate boundary segments by visual inspections of these points (Fig 2c). A plate spreading velocity of about 18.5 mm/year was found to best fit the profiles. We inverted for the locking depth of these segments, using a simulated annealing and bootstrap approach (see Figure S8 and Table S2 in the supporting information). The combination of modeled plate spreading and horizontal GIA velocities is shown in Figure 2c. The standard deviation of the residuals of the 2-km × 2-km near-East velocity grid is 3.17 mm when corrected for the updated plate boundary model, compared to 3.43 mm when corrected for the original plate boundary model and 8.44 mm when uncorrected.

4. Discussion

The high quality of our LOS velocity estimates is demonstrated by their small uncertainties, typically in the 1- to 5-mm/year range and averaging to about 2.5 mm/year (see Figures S2–S7 in the supporting information). The near-East and near-Up velocities are in good agreement with the East and Up GPS velocities (see Figures S9 and S10 in the supporting information). Their difference at the same locations gives $\sigma_{Near-East} = 2.4$ mm/year and $\sigma_{Near-Up} = 3.3$ mm/year, and there is close to one-to-one correlation.

The decomposition of the six LOS velocities fields into single near-East and near-Up velocity fields provides an important overview of deformation in Iceland. Although no ramp is removed from the initial interferograms, and each pixel is inverted independently from its neighbor during the decomposition, the resulting velocity fields show relatively small discontinuities between areas observed by a different number of tracks. We do not consider North velocities during the decomposition process, as they can lead to some biases in the estimated near-East and near-Up velocities. We estimated these eventual biases by generating synthetic East, North, and Up velocity fields based on our best fitting plate spreading and GIA models to be as close as possible to the current deformation taking place in Iceland. These velocities are then converted to LOS for each of the six satellite tracks based on heading and incidence information. The resulting six synthetic LOS velocities were then decomposed following the process described in section 2.3 to obtain near-East and near-Up velocity fields. If the decomposition process was optimal, the output near-East and near-Up velocity fields should be the same as the input synthetic East and Up velocity fields. We find that this is the case for the near-East, with less than 0.1-mm/year difference with the synthetic East, while the near-Up is more biased, with up to 1.7-mm/year difference with the synthetic Up (Figure S11 in the supporting information). These biases are, however, small with respect to the deformation rate (up to 20–35 mm/year) or the

uncertainty on the measured velocities (~2 mm/year). We also tried to invert for all three components (East, North, and Up) in areas covered by three or four tracks, but results were erroneous. North and Up velocities were unrealistically large and had canceling contributions to LOS changes. This also influenced the East velocities, which were erroneous as a result.

The GIA model used in this study removes most of the vertical velocity we observe around the edge of glaciers, especially Vatnajökull. However, some other large-scale signals remain. At the northern edge of Vatnajökull, we observe residual uplift that we relate to viscoelastic response to the dike intrusion during the 2014 Bárdarbunga rifting event (Figure 2f). We also observe residual subsidence along the plate boundary in SW Iceland. This has been observed using other geodetic techniques (Árnadóttir et al., 2009; Islam et al., 2016). Subsidence is also visible in north Iceland at the Askja, Fremri-námar, and Krafla central volcanoes and their fissure swarms. These subsidence signals have been interpreted to relate to the stretching of the crust by the plate spreading over weaker rheology (Pedersen et al., 2009).

The refined plate spreading model presented in section 3.2 explains our observations well. It uses a consistent type of observations (profiles) across all plate boundary segments, allowing better comparison between them. Each profile is inverted separately, not considering eventual influence of crustal conditions at neighboring profiles. This simplification may mask trade-offs between model parameters on neighboring profiles, in particular, in areas where the plate boundary changes direction. Nevertheless, a robust feature of the modeling is the shallow locking depth ($3.4^{+1.1}_{-0.9}$ km) in the NVZ, compared to the much greater locking depth ($10.3^{+2.8}_{-1.9}$ km) in the Eastern Volcanic Zone (EVZ), in line with the tectonic history of the rift zones as outlined by Sigmundsson, Einarsson, et al. (2018). The NVZ has been active for 6–7 million years, accommodates all the plate spreading at its latitude, and has the highest frequency of rifting events in Iceland. The EVZ is a propagating rift where activity began 2–3 million years ago, activity is propagating into older and colder crust, and time between rifting events is longer than in the NVZ. The inferred larger vertical GIA scale factor north of Vatnajökull than elsewhere, inferred from the profile studies, may also be an indication that the viscosity is less under the NVZ than EVZ, consistent with NVZ being hotter than EVZ. In the EVZ, the central axis traverses across the Hekla volcano but not Torfajökull unlike previous estimates (Geirsson et al., 2012). Its exact location there may be influenced by a local inflation source at Hekla and a deflation source at Torfajökull, not considered in the model presented here.

In the NVZ, we observe a near-Up anomaly on the Eurasian plate and the plate boundary is shifted ~20 km to the East compared to previous models. We cannot exclude that this is caused by approximation in the decomposition process, having only one ascending track covering this area. However, other data indicate that these anomalies are real. (i) The cGPS data are in good agreement with LOS velocity fields (Figures S5–S7 in the supporting information). (ii) Campaign GPS data for 2008–2014 show a similar positive vertical anomaly on the Eurasian plate, indicating the local uplift was ongoing prior to the 2014 Bárdarbunga rifting event. (iii) A regional change in East velocities during and following the 2014 Bárdarbunga rifting event is observed by most campaign GPS and cGPS in the NVZ. This anomaly in the East velocity could cause a shift of the central axis of the plate boundary model.

We observe westward directed residuals north of Bárdarbunga and eastward directed residuals north of Kverkfjöll (Figure 2e). In between is the location of the dike intrusion during the 2014 Bárdarbunga rifting event (Sigmundsson et al., 2014). This main residual signal is inferred to be due to viscoelastic relaxation of the crust following the rifting event.

Our study focuses on large-scale deformation processes, but the resolution of velocity fields is sufficient to observe small-scale deformation as well. For example, subsidence and associated contraction caused by geothermal exploitation is clearly visible on near-Up and near-East velocity fields, respectively. We observe this ongoing process at all main geothermal power plants: Reykjanes (Parks et al., 2018), Hengill (Juncu et al., 2017), and Krafla (Drouin et al., 2017). Subsidence is also observed at the following volcanoes in 2015–2018: Krísuvík, Hekla, Torfajökull, Askja, Fremri-námar, and Krafla. Öræfajökull is the only volcano showing a clear uplift during this time period. The smallest-scale identifiable deformation processes are slope instabilities, which appear to be numerous in the coastal mountain areas in North and East Iceland.

The Sentinel-1 mission has vastly improved deformation monitoring in Iceland. It provides more coverage and at a higher rate than previous SAR missions. Here we observed deformation over the entirety of Iceland (~10,0000 km^2), which indicates that it can be used to study plate dynamics in large areas. In total,

observations in 32.7 million pixels pass our coherence and outlier criteria for the 2015–2018 period. We are able to observe both large-scale signals (plate spreading, GIA) and small-scale signals (geothermal, volcano, and slope instabilities) on the same data set. This creates improved possibilities to study local deformation in the context of regional settings; confining a deformation study to the local region of interest only can lead to an underestimate or overestimate of the influence of the local source because of inadequate corrections for regional deformation fields.

5. Conclusion

Sentinel-1 images from six tracks acquired over four summers from 2015 to 2018 are successfully used to map deformation in Iceland. We used a simple approach to estimate the average LOS velocity fields for 2015–2018: single master interferometry time series together with an estimate of the linear component for each coherent pixel. LOS velocity uncertainties are about 2 mm/year. The six LOS velocity fields were decomposed to estimate the near-East and near-Up velocity fields using a process leading to no significant biases in the near-East and less than 2-mm/year biases in the vertical. Resulting near-East and near-Up velocities are in good agreement with the deformation observed by the cGPS network in Iceland; their difference gives $\sigma_{Near-East} = 2.4$ mm/year and $\sigma_{Near-Up} = 3.3$ mm/year. The near-East and near-Up velocity fields are compared to models of plate spreading and GIA. Velocities predicted by a GIA model need to be scaled up, otherwise they underestimate the current deformation field, especially in the horizontal. Residuals show that the models explain well most of the deformation. However, wide-scale deformation residuals indicate that models need further refinement, for example, taking into account a possible difference in rheology between the different rift zones in Iceland.

Acknowledgments
We thank two anonymous reviewers and the Editor for comments that helped us to greatly improve the manuscript. We acknowledge the support from the University of Iceland Research Fund and the H2020 project EUROVOLC, funded by the European Commission (Grant 731070). Collaboration and support from Landsvirkjun, the national power company of Iceland, is also acknowledged. LOS and decomposed velocity fields are available through the Open Science Framework (https://osf.io/7uxzt/?view_only=2fff37806033465385c92219c2c4a6ae). We thank the European Space Agency (ESA) for their open access policy for Sentinel SAR data. We thank the Icelandic Meteorological Office for operating the network of continuous GPS-stations in Iceland in collaboration with many institutions; data from the cGPS sites were analyzed and compared with the InSAR results. The work described here is a part of activity within the Icelandic Volcanoes permanent supersite, a part of the initiative on Geohazards Supersites and Natural Laboratories (GSNL) by the Group on Earth Observations (GEO). The intermediate TanDEM-X digital elevation model was provided by DLR under project IDEM_GEOL0123. Figures were produced with the GMT software (Wessel & Smith, 1998) and Gnuplot.

References

Altamimi, Z., Métivier, L., Rebischung, P., Rouby, H., & Collilieux, X. (2017). ITRF2014 plate motion model. *Geophysical Journal International*, *209*(3), 1906–1912. https://doi.org/10.1093/gji/ggx136

Árnadóttir, T., Lund, B., Jiang, W., Geirsson, H., Björnsson, H., & Einarsson, P. (2009). Glacial rebound and plate spreading: Results from the first countrywide GPS observations in Iceland. *Geophysical Journal International*, *177*, 691–716. https://doi.org/10.1111/j.1365-246X.2008.04059.x

Auriac, A. (2014). Solid Earth response to ice retreat and glacial surges in Iceland inferred from satellite radar interferometry and finite element modelling. (PhD dissertation), Faculty of Earth Sciences, University of Iceland.

Auriac, A., Sigmundsson, F., Hooper, A., Spaans, K. H., Björnsson, H., Pálsson, F., et al. (2014). InSAR observations and models of crustal deformation due to a glacial surge in Iceland. *Geophysical Journal International*, *198*, 1329–1341. https://doi.org/10.1093/gji/ggu205

Auriac, A., Spaans, K. H., Sigmundsson, F., Hooper, A., Schmidt, P., & Lund, B. (2013). Iceland rising: Solid Earth response to ice retreat inferred from satellite radar interferometry and visocelastic modeling. *Journal of Geophysical Research: Solid Earth*, *118*, 1331–1344. https://doi.org/10.1002/jgrb.50082

Björnsson, H., & Pálsson, F. (2008). Icelandic glaciers. *Jökull*, *50*, 365–386.

Bourbigot, M., Johnsen, H., & Piantanida, R. (2016). Sentinel-1 product definition (S1-RS-MDA-52-7440). ESA: Mission Performance Centre. DI-MPC-PB, MPC-0239, issue 2, revision 7.

Drouin, V., Sigmundsson, F., Verhagen, S., Ofeigsson, B. G., Spaans, K., & Hreinsdóttir, S. (2017). Deformation at Krafla and Bjarnarflag geothermal areas, Northern Volcanic Zone of Iceland, 1993-2015. *Journal of Volcanology and Geothermal Research*, *344*, 92–105. http://www.sciencedirect.com/science/article/pii/S0377027317303712, Volcano Geodesy: Recent developments and future challenges.

Drouin, V., Heki, K., Sigmundsson, F., Hreinsdóttir, F., & Ofeigsson, B. G. (2016). Constraints on seasonal load variations and regional rigidity from continuous GPS measurements in Iceland, 1997–2014. *Geophysical Journal International*, *205*(3), 1843–1858. https://doi.org/10.1093/gji/ggw122

Drouin, V., Sigmundsson, F., Ofeigsson, B. G., Hreinsdóttir, S., Sturkell, E., & Einarsson, P. (2017). Deformation in the Northern Volcanic Zone of Iceland 2008–2014: An interplay of tectonic, magmatic, and glacial isostatic deformation. *Journal of Geophysical Research: Solid Earth*, *122*, 3158–3178. https://doi.org/10.1002/2016JB013206

Geirsson, H., LaFemina, P., Árnadóttir, T., Sturkell, E., Sigmundsson, F., Travis, M., et al. (2012). Volcano deformation at active plate boundaries: Deep magma accumulation at Hekla volcano and plate boundary deformation in south Iceland. *Journal of Geophysical Research*, *117*, B11409. https://doi.org/10.1029/2012JB009400

Goldstein, R. M., & Werner, C. L. (1998). Radar interferogram filtering for geophysical applications. *Geophysical Research Letters*, *25*(21), 4035–4038. https://doi.org/10.1029/1998GL900033

Herring, T. A., King, R. W., Floyd, M. A., & McClusky, S. C. (2015). GAMIT reference manual : GPS analysis at MIT. (Vol. Release 10.6) [Computer software manual]. Department of Earth, Atmospheric, and Planetary Sciences Massachusetts Institute of Technology.

Islam, M. T., Sturkell, E., LaFemina, P., Geirsson, H., Sigmundsson, F., & Olafsson, H. (2016). Continuous subsidence in the Thingvellir rift graben, Iceland: Geodetic observations since 1967 compared to rheological models of plate spreading. *Journal of Geophysical Research: Solid Earth*, *121*, 321–338. https://doi.org/10.1002/2015JB012306

Juncu, D., Árnadóttir, T., Hooper, A., & Gunnarsson, G. (2017). Anthropogenic and natural ground deformation in the Hengill geothermal area, Iceland. *Journal of Geophysical Research: Solid Earth*, *122*, 692–709. https://doi.org/10.1002/2016JB013626

Keiding, M., Árnadóttir, T., Jónsson, S., Decriem, J., & Hooper, A. (2010). Plate boundary deformation and man-made subsidence around geothermal fields on the Reykjanes Peninsula, Iceland. *Journal of Volcanology and Geothermal Research*, *194*(4), 139–149. https://doi.org/10.1016/j.jvolgeores.2010.04.011

Latychev, K., Mitrovica, J. X., Tromp, J., Tamisiea, M. E., Komatitsch, D., & Christara, C. C. (2005). Glacial isostatic adjustment on 3-D Earth models: A finite-volume formulation. *Geophysical Journal International*, *161*(2), 421–444. https://doi.org/10.1111/j.1365-246X.2005.02536.x

Metzger, S., & Jónsson, S. (2014). Plate boundary deformation in North Iceland during 1992–2009 revealed by InSAR time-series analysis and GPS. *Tectonophysics*, *634*, 127–138.

Metzger, S., Jónsson, S., & Geirsson, H. (2011). Locking depth and slip-rate of the Húsavík Flatey fault, North Iceland, derived from continuous GPS data 2006-2010. *Geophysical Journal International*, *187*(2), 564–576. https://doi.org/10.1111/j.1365-246X.2011.05176.x

Pagli, C., Sigmundsson, F., Lund, B., Sturkell, E., Geirsson, H., Einarsson, P., et al. (2007). Glacio-isostatic deformation around the Vatnajökull ice cap, Iceland, induced by recent climate warming: GPS observations and finite element modeling. *Journal of Geophysical Research*, *112*, B08405. https://doi.org/10.1029/2006JB004421

Parks, M., Sigmundsson, F., Omar, S., Hooper, A., Hreinsdóttir, S., Ofeigsson, B., & Michalczewska, K. (2018). Deformation due to geothermal exploitation at Reykjanes, Iceland. *Journal of Volcanology and Geothermal Research*. https://doi.org/10.1016/j.jvolgeores.2018.08.016

Pedersen, R., Sigmundsson, F., & Masterlark, T. (2009). Rheologic controls on inter-rifting deformation of the Northern Volcanic Zone, Iceland. *Earth and Planetary Science Letters*, *281*, 14–26. https://doi.org/10.1016/j.epsl.2009.02.003

Rosen, P. A., Gurrola, E., Sacco, G. F., & Zebker, H. (2012). The InSAR scientific computing environment. In *EUSAR 2012; 9th European Conference on Synthetic Aperture Radar* (pp. 730–733). Nuremberg, Germany: VDE.

Sigmundsson, F., Einarsson, P., Ásta, R. H., Drouin, V., Jónsdóttir, K., Árnadóttir, T., et al. (2018). Geodynamics of Iceland and the signatures of plate spreading. *Journal of Volcanology and Geothermal Research*. https://doi.org/10.1016/j.jvolgeores.2018.08.014

Sigmundsson, F., Hooper, A., Hreinsdottir, S., Vogfjord, K. S., Ofeigsson, B. G., Heimisson, E. R., et al. (2014). Segmented lateral dyke growth in a rifting event at Bárdarbunga volcanic system, Iceland. *Nature*, *517*, 191–195. https://doi.org/10.1038/nature14111

Sigmundsson, F., Parks, M., Pedersen, R., Jónsdóttir, K., Ófeigsson, B. G., Grapenthin, R., et al. (2018). Chapter 11—Magma movements in volcanic plumbing systems and their associated ground deformation and seismic patterns. In S. Burchardt (Ed.), *Volcanic and igneous plumbing systems* (pp. 285–322). Amsterdam, Netherlands: Elsevier. https://doi.org/10.1016/B978-0-12-809749-6.00011-X

Vadon, H., & Sigmundsson, F. (1997). Crustal deformation from 1992 to 1995 at the Mid-Atlantic Ridge, Southwest Iceland, Mapped by Satellite Radar Interferometry. *Science*, *275*(5297), 194–197. https://doi.org/10.1126/science.275.5297.194

Wessel, P., & Smith, W. H. F. (1998). New, improved version of generic mapping tools released. *Eos, Transactions American Geophysical Union*, *79*, 579–579. https://doi.org/10.1029/98EO00426